JOURNAL OF AIRCRAFT
Vol. 43, No. 4, July–August 2006

Study of a Multitethered Aerostat System: Experimental Observations and Model Validation

Casey Lambert* and Meyer Nahon†
McGill University, Montreal, Quebec H3A 2K6, Canada
and
Dean Chalmers‡
Dominion Radio Astrophysical Observatory, Penticton, British Columbia V2A 6J9, Canada

DOI: 10.2514/1.18613

An aerial positioning system is proposed using a helium aerostat and a series of tethers attached to the ground. The system is intended to position the receiver for a large-scale radio telescope. An experimental tritethered system was developed to evaluate the behavior of the system and provide a basis for comparisons with a previously developed dynamics model. The dynamics model combines discretized lumped-mass tether models, an aerodynamic model of the aerostat and a turbulent wind model. Results from four test flights at different geometrical configurations are presented. The tritethered aerostat system exhibited impressive performance, as the payload motion was 2 orders of magnitude smaller than the aerostat motion. Validation of the dynamics model was achieved through a two-stage process. In the first step, the tether model was verified independently of the aerostat and wind models. Once the fidelity of the tether model was established, simulation results for the full dynamics model were compared to experimental results and the model proved to be effective for predicting the statistics of the motion of the system.

I. Introduction

TETHERED aerostats are passive lighter-than-air vehicles restrained by a single tether fixed to the ground. They are commonly used for positioning aerial platforms for communication, surveillance, and atmospheric sensing applications. A critical limitation of this type of system is its lack of station-keeping ability caused by its inherent passivity in response to wind input. The system is essentially at the mercy of the wind, which results in large and uncontrollable excursions. By introducing additional tethers to provide stiffness and actuation, it is possible to reduce the motions and achieve a certain level of controllability [1]. The behavior of a multitethered aerostat system has been investigated previously by the authors using a nonlinear, lumped-mass dynamics model [1,2]. The goal of this paper is to further advance the study by presenting experimental results and validation of the dynamics model.

There is little research available focusing on multitethered aerostat systems. Early experimental investigations were performed by the U.S. Air Force in 1973 [3] and by Russian meteorologists in 1978 [4]. Both studies concluded qualitatively that a tritethered aerostat system experiences much smaller displacements than that of a single-tethered system. Recently, in 2004, researchers in France performed tests on a tethered aerostat system consisting of six tethers in a double-tripod arrangement for a proposed optical telescope [5]. Although no quantitative results for the motion of the payload were presented, the concept proved feasible as astronomical observations were recorded. Slightly more research is available on experiments with single-tethered aerostat systems. The first study of a single-tethered aerostat system using modern modeling techniques was presented by Delaurier in 1972 [6]. In 1973, Redd et al. [7] developed a linear aerostat model and used a tow tank to validate it in steady wind conditions. Krausman and Jones, in 1982 [8], compared their 6-dof (degree of freedom) nonlinear model to measured results including turbulence effects and found reasonable agreement with some noticeable discrepancies. Humphreys, in 1997 [9], validated a 6-dof model of a tethered aerostat using a wind tunnel for steady state results and a tow tank for frequency response. Jones and Shroeder [10] performed a comprehensive experimental validation of a tethered aerostat model using a fully instrumented aerostat in 2001. They demonstrated good agreement between time histories of measured and simulated data for all six motion variables in response to a turbulent wind field. The present research expands on previous tethered aerostat research as it involves a quantitative experimental investigation and model validation of the dynamics of a tritethered aerostat system. This requires a full-field wind model that covers the entire tether structure as opposed to a wind input exclusively at the location of the aerostat.

The main focus of our research thus far has centered on a novel concept for a large-scale radio telescope called the Large Adaptive Reflector (LAR) [11]. The two distinct features of the LAR telescope are its reflector and the multitethered aerostat positioning system as depicted in Fig. 1. The reflector is supported by the ground and composed of many individually actuated panels that approximate a shallow paraboloid. The focal length for the reflector is 500 m, and a multitethered aerostat is proposed to support a stable aerial platform to house the receiver or feed package. Although the system displayed in Fig. 1 shows three cables in a tripod arrangement, the plan for the actual LAR telescope is to use six tethers. The steering of the telescope to observe various locations in the sky is achieved by adapting the shape of the reflector and adjusting the length of the tethers using ground winches to place the receiver at the focus of the reflector. It is also expected that the tether/winching system will be able to compensate for low-frequency wind disturbances. The study of the multitethered aerostat system has proceeded along both theoretical [1,2] and experimental avenues [12]. A dynamics model for the system was developed to estimate the motion of the system and to assist in the design process by evaluating potential design options.

II. Summary of Dynamics Model

The complete dynamics model [2] of the system consists of the following elements: 1) a discretized cable model for the three ground tethers and the aerostat leash; 2) a payload or receiver, modeled as a

Received 6 July 2005; revision received 27 February 2006; accepted for publication 27 February 2006.

*Doctoral Candidate, Department of Mechanical Engineering, Room 351, 817 Sherbrooke Street West. Student Member AIAA.
†Professor, Department of Mechanical Engineering, Room 351, 817 Sherbrooke Street West. Senior Member AIAA.
‡Research Engineer, PO Box 248.

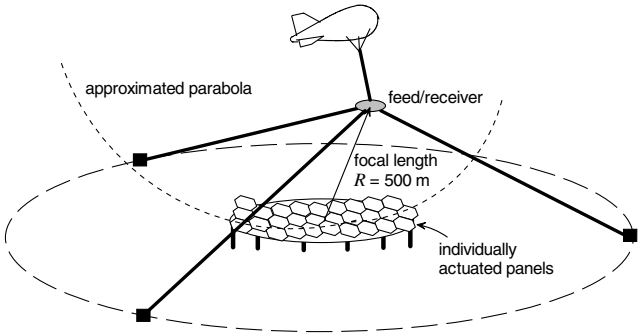

Fig. 1 Schematic diagram of LAR radio telescope concept consisting of a panel-segmented reflector and a multitethered aerostat feed positioning system.

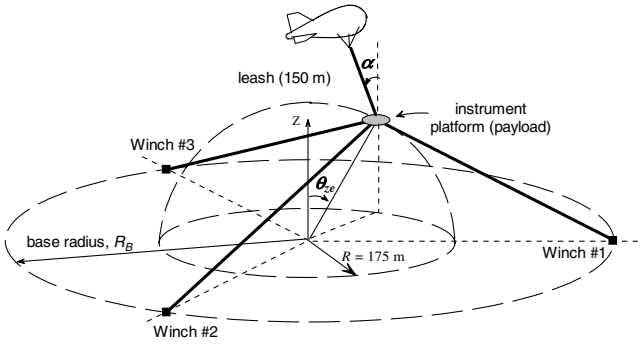

a)

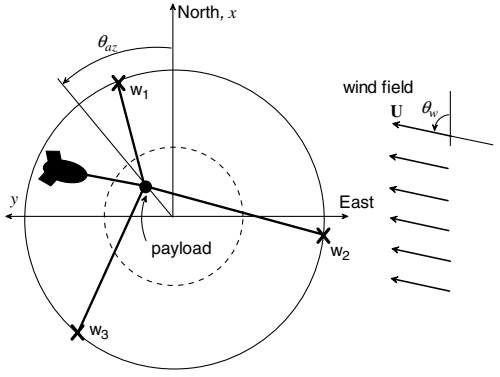

b)

Fig. 2 a) Layout of experimental tritethered aerostat system, b) top view.

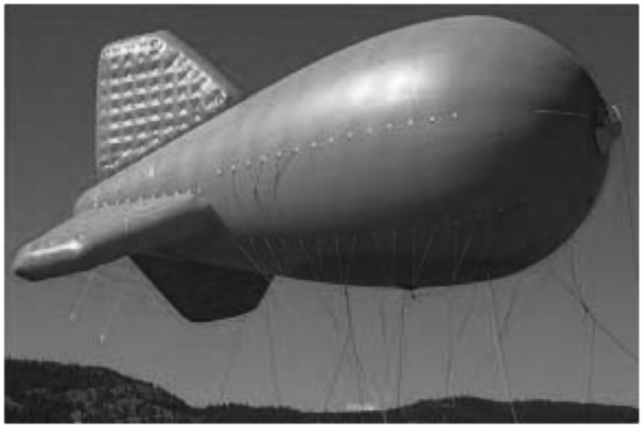

Fig. 3 Worldwide Aeros 18 m aerostat.

simple spherical shell; 3) an aerodynamics model of a streamlined aerostat; and 4) a full-field wind model, including turbulence.

The cable model is based on the discretization of each tether into individual elements, which are considered lumped masses or nodes interconnected by viscoelastic elements [1]. The forces acting on each node are external—aerodynamic and gravity, and internal—elastic and damping. For all the simulations presented here, each tether was discretized into 10 elements.

The aerodynamics rigid body model of the aerostat [2] was achieved by separating it into three components: the flying harness, the tail fins and the hull, and approximating the aerodynamic properties of each component separately. The fins were modeled as NACA 0018 airfoils with a low aspect ratio. The hull geometry was used with empirical data [13] to estimate its aerodynamic coefficients, and the flying harness was included as a single drag force based on the sum of the total cross-sectional area of its constituent cables.

The wind was modeled using a mean wind speed superimposed with turbulent gusts. The mean wind U varies with height h according to the following power law profile representing the Earth's boundary layer [14]:

$$U = U_g \left(\frac{h}{h_g} \right)^{\gamma} \tag{1}$$

where the power law exponent, $\gamma = 0.30$ and the boundary layer height, $h_g = 500$ m were used to represent the region's hilly terrain [14]. U_g is the full wind speed above the boundary layer. The turbulence is generated with desired gust statistical properties [15], including turbulence intensity [16], scale length, and a von Kármán spectrum.

The dynamics of each discretized tether node and the payload node are described by 3 second-order ordinary differential equations (ODEs) obtained using Newton's translational motion equations. For the aerostat, three additional ODEs derived from Euler's rotational motion equations are required. In total, 234 first-order ODEs are needed to describe the complete system with each tether discretized into 10 elements. The motion of the system is obtained by simultaneously solving the ODEs using a fourth order Runge–Kutta numerical integration routine. The right-handed inertial coordinate frame for all simulations is shown in Fig. 2b.

III. Experimental System Description

The experimental analysis of the multitethered aerostat system was addressed by constructing a one-third scale prototype at the Dominion Radio Astrophysical Observatory (DRAO) in Penticton, British Columbia [12]. The objective of the scaled prototype is to provide results to validate the dynamics model and to address pertinent operational and logistical concerns. The choice of scale factor was a compromise between cost and accuracy of results. A scale factor close to unity would ensure that the prototype results would be closer to those of the full-scale system, whereas a smaller scale factor would allow the system to be constructed at lower cost and allow greater ease of experimentation.

The main components of the experimental system are a helium aerostat, three tethers with winches, and an instrumentation platform as shown in Fig. 2. Details of the design of the experimental system are provided in [12]. The LAR telescope requires that the payload be positioned at all points on a hemisphere with a zenith angle, θ_{ze}, between 0 and 60 deg. The radius of the hemisphere for the scaled system is about 175 m. Winches can be used to adjust the tether lengths to move the payload to different configurations.

A streamlined aerostat was chosen for the experiment because its drag is expected to be 3 to 4 times lower than a spherical aerostat. The aerostat, shown in Fig. 3, is inflated with helium and was manufactured by Worldwide Aeros. The maximum net lift is 260 kg, however, due to helium contamination the actual lift is usually less. The tethers are manufactured by Cortland Cable and are made of *Plasma*, a light, high strength, high-stiffness braided rope made from ultrahigh molecular weight polyethylene. A high strength-to-weight

Table 1 Characteristics of aerostat and tethers

Aerostat		Tether	
Diameter	7.7 m	Diameter	6 mm
Length	18 m	Density	840 kg/m^3
Volume	530 m^3	Young's mod.	37.4 GPa
Fineness ratio	2.4	Length	100–500 m
Max net lift	260 kg	Damping ratio	0.017

ratio is critical for the tethers as it limits the amount of sag for a particular tension (tether sag significantly reduces the stiffness of the tension structure). The characteristics of the aerostat and the tethers are given in Table 1. The tether lengths vary depending on the configuration of the system.

The upper tether connecting the instrument platform to the aerostat is referred to as the *leash* and it has the same characteristics as the other tethers. It has a fixed length of 150 m and also contains conductors that are used to transmit power and data to the aerostat. An additional tether (not shown in Fig. 2), which remains slack during all tests, connects the instrument platform to the ground. This cable allows system deployment and retrieval and permits high-speed data transfer from the airborne instrument platform.

The instrument platform, shown in Fig. 4, is a 0.8 m circular plate attached to the three ground tethers by Teflon-coated hangers. Mounted on the plate are a global positioning system (GPS) antenna and receiver, a two-axis tilt sensor, a digital compass, and a two-axis ultrasonic wind sensor. An S-type load cell is incorporated at the top of each of the tethers and the leash to measure cable tensions. This suite of sensors thus allows a complete and precise knowledge of the motion and forces at the confluence point. In addition to the above, the aerostat has its own set of sensors, including a GPS antenna and receiver, a two-axis tilt sensor and a digital compass. Finally, mounted at reference ground locations, we have a third GPS antenna and receiver used as a base reference for differential GPS measurements of the two airborne units.

All sensors are analog, and their data are digitized on the platform at a rate of 10 Hz. The GPS data are transmitted via an onboard radio modem, whereas the remaining data are transmitted to the ground through conductors in the central tether, using an RS-485 protocol.

IV. Flight Tests

Four test flights were performed at the DRAO facility in Penticton, British Columbia during the spring of 2004. The purpose of the flights was to study the passive or uncontrolled performance (winches turned off) of the tritethered aerostat system and to assess the quality of our dynamics model. Tests were performed at two different tether base radii R_B and two different payload locations (different zenith and azimuth angles) to investigate how changes in tether geometry affect the behavior of the system. Table 2 gives a summary of the tether configuration for the four flights. The focal length (distance from the center of the base circle to the confluence point) for the flights was approximately 175 m and the aerostat leash length (from confluence point to aerostat) was 150 m. The net lift for the aerostat changes with each flight depending on the purity of helium in the envelope and the atmospheric conditions. Results for the four flights are summarized in Table 3. The position of the aerostat and the platform were obtained from differential GPS sensors, which have circular error precision (CEP) of 1 cm.

The system's station keeping abilities are evaluated by considering the standard deviation of the platform motion. With the exception of flight 2, which was at an unfavorable configuration, the system proved to be effective as demonstrated by platform motion on the order of 5 cm horizontally and 10 cm vertically. The efficacy of the system is also made apparent by the significant reduction in horizontal motion between the aerostat and the platform. During flights 1 and 4, which are both at favorable low zenith angles, the standard deviation of the horizontal motion of the platform was 2 orders of magnitude smaller than the aerostat motion. Vertical motion was also smaller at the platform but the improvement was much less marked. Figure 5 gives plots for the motion of both the platform and the aerostat during flight 4. There is obvious correspondence between the motions of the two bodies in the x and y horizontal directions with the platform lagging the aerostat very slightly. In the vertical z direction, the motion of the platform and the aerostat are of the same order of magnitude.

Figure 6 displays the coherence between the motion variables of the two bodies in the x, y, and z directions. The coherence function $C_{ab}(f)$ of two real-valued signals $a(t)$ and $b(t)$ for a specific frequency f is given by

Table 2 Summary of test flights

	No. 1 March 11	No. 2 March 23	No. 3 April 21	No. 4 June 15
Base radius, R_B, m	250	250	400	400
Zenith, θ_{ze}, deg	2	29	29	2
Azimuth, θ_{az}, deg	−101	−40	−40	−101
Platform height, m	175.4	155.7	150.2	172.8
Aerostat net lift, kg	195	175	186	237

Table 3 Test results for wind speed, turbulence intensity, aerostat and platform motion (standard deviation), and tether tensions

		No. 1 March 11	No. 2 March 23	No. 3 April 21	No. 4 June 15
Mean wind, U,m/s		4.94	4.49	3.15	3.75
Mean wind direction		185	2.03	174	185
Turbulence intensity, σ_U/U		0.14	0.06	0.10	0.16
Horizontal motion, m	σ_{aerostat}	4.26	3.31	2.63	3.32
	σ_{platform}	0.031	0.93	0.060	0.030
	% reduction	99.3	71.9	97.7	99.1
Vertical motion, m	σ_{aerostat}	0.411	0.219	0.170	0.134
	σ_{platform}	0.093	0.207	0.077	0.095
	% reduction	77.4	5.5	54.7	29.1
Leash mean tension, N		2473	1849	1897	2627
Tether 1 mean tension, N		1309	1036	1356	1238
Tether 2 mean tension, N		975	913	1287	1193
Tether 3 mean tension, N		805	173	717	1091

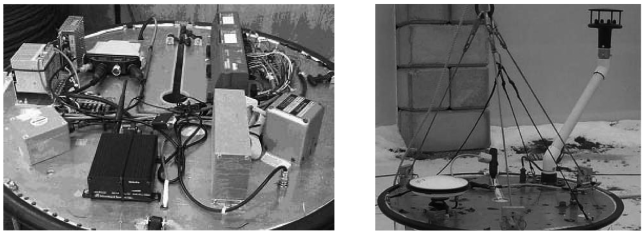

a) b)

Fig. 4 Instrument platform a) underside with sensors and A/D converters, b) top side with GPS antenna and wind sensor.

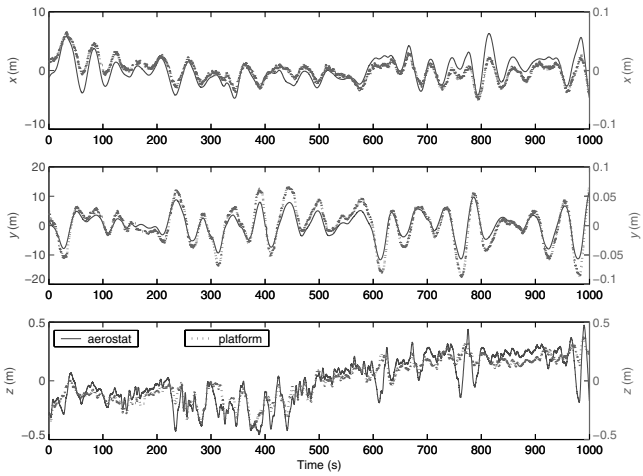

Fig. 5 Motion of aerostat (left axis, solid line) and instrument platform (right axis, dotted line) about their mean positions during flight 4.

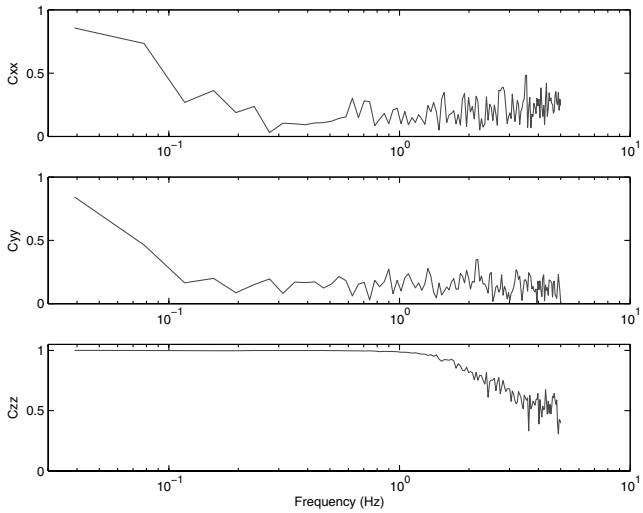

Fig. 6 Coherence between aerostat position and platform position for flight 4.

$$C_{ab}^2(f) = \frac{|P_{ab}(f)|^2}{P_{aa}(f)P_{bb}(f)} \tag{2}$$

where $P_{ab}(f)$ is the cross-power spectral density of the two signals, and $P_{aa}(f)$ and $P_{bb}(f)$ are the power spectral densities of a and b, respectively. The coherence function, which ranges from zero to one, quantifies the correlation of two signals over a range of frequencies. A coherence of zero indicates incoherent signals, whereas a value of 1 indicates full coherence or correlation. Horizontally, there is coherence at only the lowest frequencies (observed in the time histories in Fig. 5), and above 0.1 Hz there is negligible coherence. Vertically, there is strong coherence between the two bodies beyond 1 Hz. The coherence plots clearly demonstrate the tritethered system's ability to filter out all but low-frequency horizontal motions, while highlighting its inability to filter out any vertical motions below 1 Hz.

It would be difficult to directly compare the performance of the four different geometric configurations tested because several influential factors were not controlled such as wind speed, turbulence intensity, and aerostat lift. However, it is still possible to make qualitative observations regarding the relative performance of these configurations. It is clear that the worst performance was observed during flight 2, which was tested at a small base radius and high zenith angle. This geometry considerably reduced the stiffness of the system by two different mechanisms. First, the structural stiffness of the tripod is reduced in certain directions due to the asymmetry of the system. Secondly, the tether asymmetry causes tension to drop in one tether, thus increasing its catenary, or sag, and reducing its effective stiffness. During flight 2, the mean tension in tether 3 was only 173 N and the standard deviation of the horizontal displacement of the platform was almost 1 m, whereas for all other flights it was less than 6 cm. It should be mentioned that the net lift of the aerostat was lowest during this flight, which also contributed to the poor performance.

To ensure adequate performance of the system, a certain tension level must be maintained in all tethers at all times. Increasing the lift of the aerostat is one suitable method to achieve this, although not practical for our experiments, but a second, more practical, solution is to increase the base radius R_B. The larger base radius of 400 m significantly improved the performance of the system at high zenith angles as observed comparing results of flight 2 and of flight 3.

For the tests near the zero zenith, flights 1 and 4, the wider base radius is observed to reduce the stiffness in the vertical direction while having little effect on the horizontal stiffness. The relative stiffness is qualitatively evaluated by considering the percent reduction of motion between the aerostat and the platform.

Overall, the test results show that precise station keeping is possible with a tritethered aerostat system as a 40 kg platform was held to within 10 cm rms error at heights ranging from 150 to 175 m. The geometry of the tether layout was shown to significantly affect performance of the system and the importance of maintaining sufficient tension in all tethers was highlighted. Optimizing design parameters such as aerostat lift, tether material properties and size, geometry, and the number of base tethers could likely enhance performance further.

The preliminary design specifications for the functioning LAR telescope call for maintaining a receiver position within 1 cm rms of the receiver focus. A mechanism will be installed at the confluence point to perform fine corrections, and the requirements on the cable system are for a precision of less than 0.5 m rms which translates to 17 cm for our scaled system. Our results suggest that the system should be able to deliver the precision required, but the limited number of conditions tested precludes definitive claims about performance of the telescope at this time.

V. Validation of the Tether Model

It is possible to validate the tether model in isolation from the aerostat model, and by first establishing the accuracy of the tether model, the validation of the complete model becomes more straightforward. The tether model can be directly compared to the flight test results by removing the aerostat, in the dynamics model, from the top of the leash and replacing it with the *measured* leash force during a particular flight (the load cell measuring leash tension is located at the aerostat leash attachment point). The direction of the force is estimated along the position vector from the platform to the aerostat obtained using GPS measurements. The estimated effects of the wind on the platform structure and the tethers, although small compared to the aerostat force transmitted through the leash, were also included in the simulation results.

A comparison of the flight data and simulated results (using measured leash tensions to replace the aerostat) is presented in Table 4. The percentage differences between the standard deviation

Table 4 Percentage difference between the standard deviation of experimental data and simulated data using measured leash force

		No. 1 March 11	No. 2 March 23	No. 3 April 21	No. 4 June 15
Platform position	Horizontal	2.4	−1.6	3.8	−5.4
	Vertical	−20.8	0.7	−3.7	−11.4
Tether 1 tension		−2.6	0.4	1.2	−1.9
Tether 2 tension		0.9	0.2	3.0	3.1
Tether 3 tension		3.8	3.4	4.3	2.4

of the experimental and simulated platform motion and tether tensions are given. The results for flight 3 are presented in Fig. 7 to illustrate how well the tether model predicts the platform motion when using the measured leash tension as input. The discrepancy in the z direction is believed to be caused by creep in the tethers. This effect is not included in the model but it was observed on all four flights. For all calculations of the standard deviation of the experimental vertical motion, the creep rate was disregarded by removing the linear trend from the data. Creep is not expected to be a problem with functioning winches as the creep rate of approximately 0.1 mm/s can be corrected easily.

The values for the tether tension and horizontal motion are all within 6%, which is indicative of a satisfactory tether model. For the vertical motion, the percentage difference is as large as 21%; however, the values for the standard deviation of the measured vertical motion may be skewed slightly due to the observed creep. Although a linear trend is removed from the motion before the calculation, if the creep rate is not constant, the standard deviation of the measured results will be exaggerated.

VI. Complete Model Validation

Results are now presented for the complete dynamics model of the system. The statistics of the measured wind conditions for each particular flight were provided as input to the model and the motion of the system was estimated and compared to the actual measured data. Because the wind speed was measured 150 m below the aerostat, the precise wind field in the vicinity of the aerostat is unknown. This limits the precision of our validation effort, as a direct temporal comparison to experimental data is not possible. The modeled wind field, for our simulation, is spatially extrapolated from the measurement platform based on statistical approximations of the actual wind conditions. Because the wind speed at the aerostat, which is responsible for the majority of the disturbances in the system, is modeled based on a statistical approximation of the actual wind field, the validation of the dynamics model must be based on statistical results.

The following steps were taken to ensure that the wind field in the simulation was statistically similar to that in the field:

1) The low-frequency characteristics of the wind were approximated by fitting a curve to the general trend of the wind speed at its measurement height.

2) The vertical profile of the basic wind field was generated using a power-law boundary layer profile, as discussed in Sec. II.

3) The mean wind direction was estimated by averaging the mean wind-sensor measurement at the platform and the mean yaw angle of the aerostat.

4) Turbulent gusts were superimposed on the basic wind field, which are approximated using von Kármán spectra [1] based on the measured turbulence intensity for the test period. The vertical profile of the turbulence intensity, which decreases with height, is extrapolated from the measurement location using empirical relationships [16].

One limitation of this approach is that only the horizontal component of the wind speed is measured and thus the vertical turbulence is unknown. Although the vertical component of the wind is not expected to be large, it can have a significant impact on the motion of the aerostat [7]. An estimate of the vertical component of turbulence, relative to the measured horizontal turbulence levels and with an empirically obtained vertical profile [16], is included in the model. However, because no vertical wind speed measurements are available, there is considerable uncertainty in our results pertaining to possible updrafts or downdrafts.

The frequency content of the measured and simulated turbulence is compared in Fig. 8, which gives the power spectral densities in directions along and perpendicular to the mean wind direction. For brevity, only results for flights 1 and 3 are presented. The simulated turbulence appears to have the approximate characteristics of the measured turbulence throughout the bandwidth of our sensor, but it is clear that the turbulence model does not always recreate the actual wind spectrum, which varies significantly day to day. The drop-off at high frequencies in the spectra for both experimental and simulated wind data adhere to the expected $-5/3$ slope for isotropic turbulence [17]. The spike in the experimental data of the lower plot is the result of a cooling fan onboard the platform that causes small amplitude vibrations.

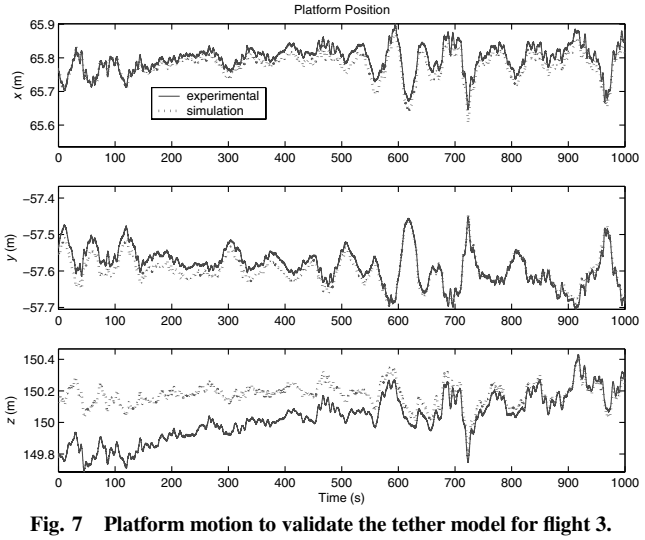

Fig. 7 Platform motion to validate the tether model for flight 3.

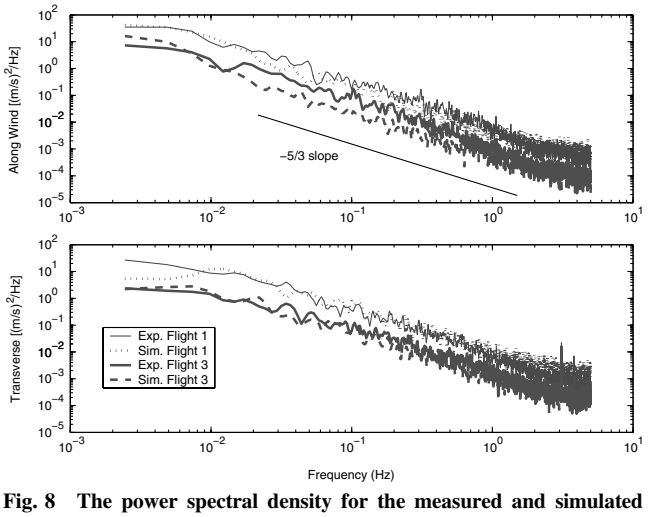

Fig. 8 The power spectral density for the measured and simulated horizontal turbulence along the wind direction and transverse to it for flights 1 and 3.

Table 5 Comparison of experimental and simulated results for flights 1 and 3

Measured parameter		Flight 1 March 11			Flight 3 April 21		
		Exp.	Sim.	% diff.	Exp.	Sim.	% diff.
Platform position, m	σ_x	0.021	0.020	−6.7	0.039	0.047	19.8
	σ_y	0.030	0.048	60.7	0.042	0.044	3.2
	σ_z	0.093	0.085	−8.4	0.077	0.105	37.2
Aerostat position, m	x	−19.94	−15.67	21.4	62.26	57.43	−7.8
	y	−9.85	−7.17	27.2	−58.82	−56.48	−4.0
	z	337.36	337.73	0.1	312.66	312.57	0.03
	σ_x	3.13	2.86	−8.6	2.33	1.28	−45.1
	σ_y	5.09	7.68	51.0	4.76	3.15	−33.8
	σ_z	0.411	0.388	−5.6	0.170	0.150	−11.4
Leash angle aerostat rotation, deg	α	6.9	5.7	−17.6	1.9	3.1	61.6
	σ_ϕ	2.11	2.35	11.0	1.70	0.95	−44.2
	σ_θ	1.10	0.96	−13.0	0.59	0.40	−31.6
	σ_ψ	5.24	4.77	−9.1	11.78	2.41	−79.5
Tether tension, N	T_{leash}	2473	2220	−10.2	1897	1882	−0.9
	σ_{leash}	182	190	4.3	35	50	42.7
	σ_{T1}	124	130	5.4	46	55	42.7
	σ_{T2}	126	136	7.7	51	61	19.5
	σ_{T3}	89	113	26.5	30	33	8.8

Table 5 presents a comparison of the measured and simulated data for platform position, aerostat position and rotation, and tether tension. For all parameters except the aerostat position and leash tension, the mean values are omitted and only a comparison of the standard deviation is presented. Flights 1 and 3 were chosen for the comparison because they represent the contrast of the validation results. For flight 1, the simulation predicts well the platform motion in the aerostat longitudinal directions while overestimating the motion in the lateral direction and for flight 3, the opposite is true. For all the test flights, the predominant wind direction was north, which is aligned with the x axis of our inertial frame. Thus, the lateral motion of the aerostat is represented by motion in the y direction along with the aerostat roll φ and yaw ψ whereas the longitudinal motion is described by motion in the x and z directions as well as aerostat pitch θ.

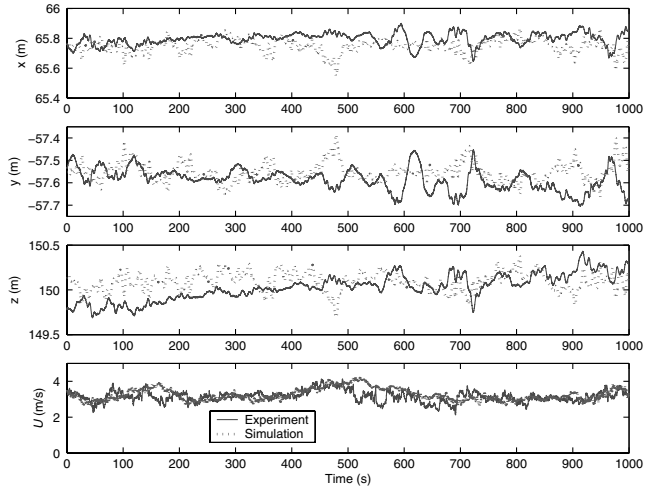

Fig. 9 Comparison of experimental and simulated results of platform position and wind speed for flight 3.

Figures 9–11 compare time histories of measured and simulated results for flight 3. It must be emphasized that the simulated results are not expected to directly follow the measured results because the simulated wind turbulence was based only on the statistical properties of the measured wind, not on the wind's precise time history and because the wind is measured 150 m below the aerostat. The goal of comparing time histories is to provide a general assessment of the simulation's effectiveness.

For flight 3, the simulation estimates of the horizontal platform motion are within 20% of the actual results, which is encouraging considering this corresponds to accuracy of less than a centimeter. For flight 1, the predicted platform motion differs by as much as 60% in the lateral or y direction, which seems large, however, this corresponds to a difference in motion of less than 2 cm. Considering the size of the positioning system: the platform is 175 m high,

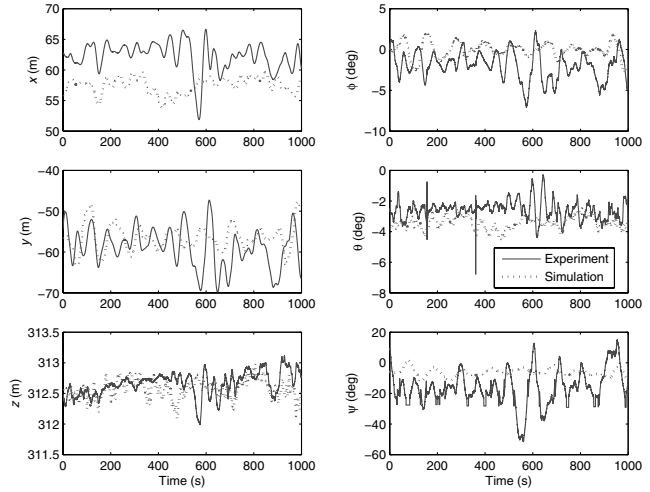

Fig. 10 Comparison of experimental and simulated results for aerostat position and rotation for flight 3.

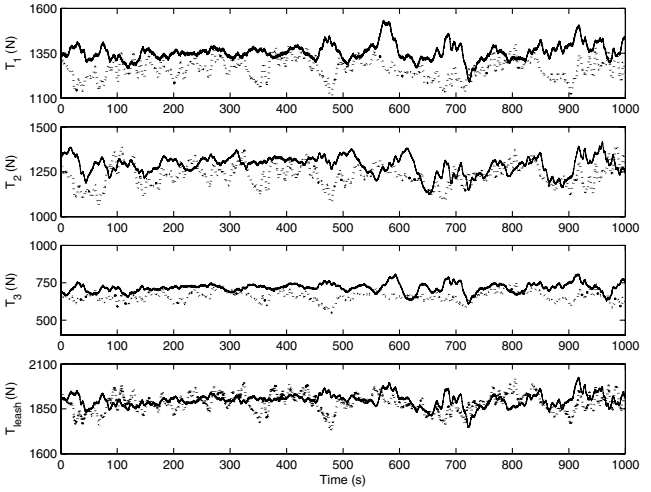

Fig. 11 Comparison of experimental and simulated results for tether tension for flight 3.

anchored by tethers hundreds of meters long; a 2 cm discrepancy is more than satisfactory. There are several instances where our simulated results diverge from the measurements but the differences do not appear to be consistent across all the test cases. During flight 1, the simulation overpredicted the lateral motion of the platform by 60% whereas the variation in yaw was within 10%. The reverse is observed during flight 3, as the standard deviation of the aerostat yaw angle differs by 80% whereas the lateral motion is predicted to within 5%.

In terms of the longitudinal motion of the aerostat, it is observed in Fig. 10 that during flight 3, the simulated aerostat position in the x direction is 4 m less than measured corresponding to a larger blow-down angle, or leash angle α in the simulation, suggesting that either the wind speed or the drag coefficient or both are overestimated. Conversely, during flight 1, the leash angle α measured from the vertical of the simulated results is less than the measured values suggesting that the wind speed or drag coefficient is underestimated. It is likely that the wind model and the aerodynamics model of the aerostat will both contain inaccuracies because the wind input to the aerostat is based on statistical approximations of measurements 150 m below the aerostat and the aerostat model contains several approximations based on empirical data [2]. However, unless more precise knowledge of the actual wind conditions near the aerostat is obtained, it is imprudent to develop an explanation for the model's divergence. Instead, the limitations of the simulation must be recognized and the results interpreted accordingly.

The power spectra of the experimental and simulation results for leash tension, horizontal and vertical platform motion for flight 3 are shown in Fig. 12. For the two motion plots, a third spectral density is given for the simulation results of the previous section using the measured leash force in place of the aerostat model. The simulated leash tension has a slightly larger magnitude over most of the bandwidth, but the similarity of the peaks through the midrange of frequencies indicates that the model captures most of the important modes affecting the leash tension. There is a noise floor for each of the measured quantities that prevent comparison at high frequencies. However, the simulation appears to have some high frequency peaks that were not measured during the flight. The peak in the simulated leash tension at 2 Hz suggests that a particular oscillation is overemphasized in the model, but the magnitude is small enough that it is not expected to have much impact on the statistical validation in Table 5.

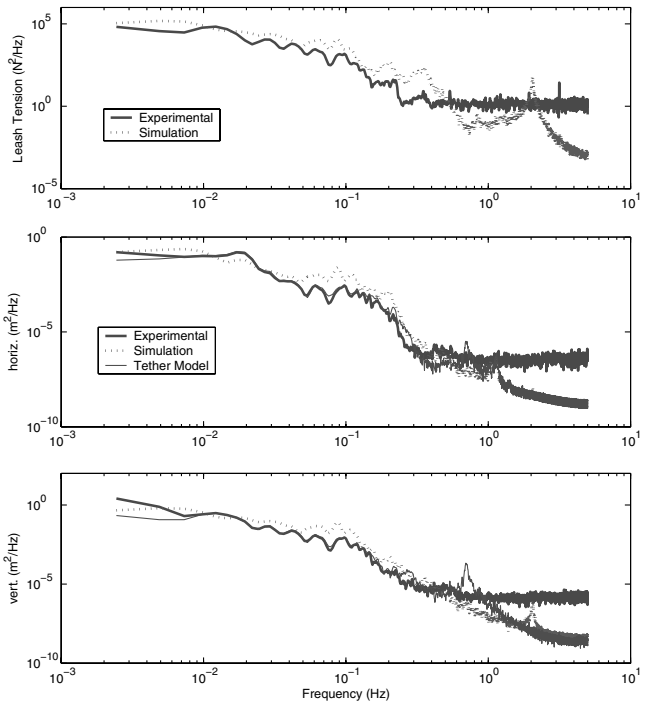

Fig. 12 Power spectral density of experimental and simulated leash tension, horizontal, and vertical platform motion for flight 3.

The results for the vertical motion of the tether model show excellent agreement with the experimental results, except at the lowest frequency and at a spike at about 0.7 Hz. The low-frequency discrepancy is due to tether creep, observed in Fig. 7, but the source of the spike at 0.7 Hz is not clear. The magnitude of the peak is small enough to not significantly affect the results as good statistical agreement between the tether model and the flight data can be seen in Fig. 7 and Table 4.

VII. Conclusion

The effectiveness of a tritethered aerostat positioning system was demonstrated during experimental trials. The horizontal motion of the platform was reduced by as much as 2 orders of magnitude over the ensuing motion of the aerostat. The stiffness of the system decreased when positioning the platform on a hemisphere at zenith angles near 30 deg, but the stiffness improved when the tethers were spread out radially.

The dynamics model for the system was validated in two stages: the first stage was to validate the tether model alone using the measured aerostat leash tension to drive the system, and the second stage consisted of a statistical and frequency response comparison between the experimental results and the simulation results of the complete model, including an aerodynamics model of the aerostat and a turbulence model of the wind. The tether model proved effective as simulated results for the tether tension and horizontal motion were within 6% of measured values for all four flights, whereas variations in the vertical displacement, affected by tether creep, varied by as much as 21%. The accuracy of the complete dynamics model was demonstrated by analyzing results for two flights representing the range of results for the four spring 2004 flight tests. The standard deviation of simulated platform motion was overestimated to within 3 cm of the measured response of both flights. Considering the scale of the system, these results meet our expectations for the dynamics model and create a basic level of confidence that the model is capable of predicting realistic behavior for a prescribed wind condition. The validation of the model, based on statistical similarity to experimental data, is limited by our incomplete knowledge of the governing wind conditions.

Acknowledgments

The authors gratefully acknowledge the financial support received from the Natural Sciences and Engineering Research Council of Canada, the Canada Foundation for Innovation, and the National Research Council of Canada.

References

[1] Nahon, M., "Dynamics and Control of a Novel Radio Telescope Antenna," *Proceedings of the AIAA Modeling and Simulation Technologies Conference and Exhibit*, AIAA, New York, 1999, pp. 214–222.

[2] Nahon, M., Gilardi, G., and Lambert, C., "Dynamics and Control of a Radio Telescope Receiver Supported by a Tethered Aerostat," *AIAA Journal of Guidance, Control and Dynamics*, Vol. 25, No. 6, 2002, pp. 1107–1115.

[3] Leclaire, R. C., and Rice, C. B., "The Local Motions of a Payload Supported by a Tritethered Natural Shape Balloon," U.S. Air Force, Rept. AFCRL-TR-73-0748, Dec. 1973.

[4] Masterskikh, M. A., "A Method for Holding a Pilot Balloon or Light Aerostat at a Predetermined Height for Meteorological Observations," *Meteorologiya i Gidrologiya*, No. 4, 1978, pp. 102–104.

[5] Le Coroller, H., Dejonghe, J., Arpesella, C., Vernet, D., and Labeyrie, A., "Tests With a Carlina-type Hypertelescope Prototype," *Astronomy and Astrophysics*, Vol. 426, No. 2, 2004, pp. 721–728.

[6] DeLaurier, J. D., "A Stability Analysis for Tethered Aerodynamically Shaped Balloons," *AIAA Journal of Aircraft*, Vol. 9, No. 9, 1972, pp. 646–651.

[7] Redd, T., Bland, R., and Bennett, R. M., "Stability Analysis and Trend Study of a Balloon Tethered in a Wind, with Experimental Comparisons," NASA TN D-7272, Langley Research Center, Oct. 1973.

[8] Jones, S. P., and Krausman, J. A., "Nonlinear Dynamics Simulation of a Tethered Aerostat," *AIAA Journal of Aircraft*, Vol. 19, No. 8, 1983, pp. 120–126.

[9] Humphreys, D. E., "Validation of the Dynamics Characteristics of a Towed, Scaled Aerostat," *Proceedings from the 12th AIAA Lighter-Than-Air Systems Technology Conference*, AIAA, New York, 1997, pp. 227–236.

[10] Jones, S. P., and Shroeder, L. D., "Nonlinear Dynamics Simulation of a Tethered Aerostat: A Fidelity Study," *AIAA Journal of Aircraft*, Vol. 38, No. 1, 2001, pp. 64–68.

[11] Fitzsimmons, J. T., Veidt, B., and Dewdney, P., "Steady-State Stability Analysis of the Multi-Tethered Aerostat Platform for the Large Adaptive Reflector Telescope," *Proceedings of the SPIE International Symposium on Astronomical Telescopes and Instrumentation*, International Society for Optical Engineering, Bellingham, WA, 2000, pp. 476–487.

[12] Lambert, C., Saunders, A., Crawford, C., and Nahon, M., "Design of a One-Third Scale Multi-Tethered Aerostat System for Precise Positioning of a Radio Telescope Receiver," *Proceedings of the Canadian Aeronautics and Space Institute Flight Mechanics and Operations Symposium*, AIAA, New York, 2003.

[13] Jones, S. P., and DeLaurier, J. D., "Aerodynamic Estimation Techniques for Aerostats and Airships," *AIAA Journal of Aircraft*, Vol. 20, No. 2, 1983, pp. 120–126.

[14] Davenport, A. G., "Rationale for Determining Design Wind Velocities," *American Society of Civil Engineers Journal of Structural Division*, Vol. 86, No. ST5, May 1960, pp. 39–68.

[15] Etkin, B., *Dynamics of Atmospheric Flight*, Wiley, New York, 1972, pp. 529–543.

[16] Engineering Sciences Data Unit, "Characteristics of Atmospheric Turbulence Near the Ground," Pt. 2 ESDU Item 74031, London, England, 1974.

[17] Houbolt, J. C., "Atmospheric Turbulence," *AIAA Journal*, Vol. 11, No. 4, 1972, pp. 421–437.